

Breakdown of inverse morphologies in charged diblock copolymers

Monojoy Goswami,^{*,†} Rajeev Kumar,[‡] Bobby G. Sumpter,[†] and Jimmy Mays[†]

Oak Ridge National Laboratory, Oak Ridge, TN, 37831, National Center for Computational Sciences, Oak Ridge National Laboratory, Oak Ridge, TN, 37831, and Department of Chemistry, University of Tennessee, Knoxville, TN, 37996

E-mail: goswamim@ornl.gov

*To whom correspondence should be addressed

[†]Oak Ridge National Laboratory, Oak Ridge, TN, 37831

[‡]National Center for Computational Sciences, Oak Ridge National Laboratory, Oak Ridge, TN, 37831

[¶]Department of Chemistry, University of Tennessee, Knoxville, TN, 37996

October 25, 2018

Abstract

Brownian Dynamics simulations are carried out to understand the effect of temperature and dielectric constant of the medium on microphase separation of charged-neutral diblock copolymer systems. For different dielectric media, we focus on the effect of temperature on the morphology and dynamics of model charged diblock copolymers. In this study we examine in detail a system of partially charged block copolymer consisting of 75% neutral blocks and 25% of charged blocks with 50% degree of ionization. Our investigations show that due to the presence of strong electrostatic interactions between the charged block and counterions, the block copolymer morphologies are rather different than their neutral counterpart at low dielectric constant, however at high dielectric constant the neutral diblock behaviors are observed. This article highlights the effect of dielectric constant of two different media on different thermodynamic and dynamic quantities. At low dielectric, the morphologies are a direct outcome of the ion-counterion multiplet formation. At high dielectric, these charged diblocks behavior resembles that of neutral and weakly charged polymers with sustainable long-range order. Similar behavior has been observed in chain swelling, albeit with small changes in swelling ratio for large change in polarity of the medium. The results of our simulations agree with recent experimental results and are consistent with recent theoretical predictions of counterion adsorption on flexible polyelectrolytes.

Introduction

Microphase separation in neutral-neutral diblock copolymer melts and solutions has been studied extensively during the last two decades.¹⁻⁵ However, self-assembly of amphiphilic macromolecules still eludes a clear understanding. Despite the importance of these molecules for a number of technological and biological applications, a large parameter space affecting the self-assembly process poses serious problems for the scientific community.

In particular, an amphiphilic diblock copolymer containing a charge block attached to a neutral block is of great importance to a large classes of nanotechnology applications⁶⁻¹² and drug-delivery systems.¹³⁻¹⁸ Pioneer experiments on the self-assembly of amphiphilic copolymers in solutions by Eisenberg and his coworkers¹² have revealed that different morphologies can be obtained by varying the composition of polystyrene (PS)-*b*-poly(acrylic acid) (PAA). In addition to the three well-known classical morphologies, namely, spheres, cylinders or rods and lamellae, two more morphologies were discovered. These two morphologies included vesicles in aqueous solution and simple reverse micelle-like aggregates in organic solvents.

Origin of these morphologies (or micelles) in the context of amphiphilic copolymer solutions has been investigated extensively.^{1,2,4,19} General consensus is that the micellization/aggregation of an amphiphile results from a balance between three different contributions to the free energy: chain stretching in the core, the interfacial energy and the repulsion/attraction between the coronal chains.²⁰ However, the presence of charges in the case of charged-neutral diblock copolymers complicates this simple picture of the balance of forces and sometimes, leads to non-trivial counter-intuitive morphologies. For example, for a particular set of parameters, stacking disk-shape structures have been observed experimentally.^{11,19,21} As an another example, in a system consisting poly(acrylic acid-*b*-styrene) (PAA-*b*-PS) diblock copolymer, disk-shape one dimensional supra-assembly have been formed in a controlled manner.^{11,21}

To understand the structures and the mechanisms by which amphiphilic diblock copolymers self-assemble into different morphologies, a comprehensive theoretical/simulation study is necessary. However, theoretical work on the ordered morphologies of amphiphilic block copolymers is relatively scarce.²²⁻²⁵ The few theoretical studies of diblock amphiphiles and triblock copolymers that have been conducted to understand the formation of self-assembled structures includes molecular dynamics (MD),²⁶⁻²⁸ Monte Carlo (MC)²⁹⁻³¹ and self-consistent field theory (SCFT).^{32,33} Although most of these recent simulation studies address self-assembly in solution,^{24,25} recently there have been efforts to approach the problem using dissipative particle dynamics (DPD) to understand the mesoscopic self-assembly of amphiphilic block copolymers in polymer melts.³⁴⁻³⁷ In

solution, Guo *et.al.*^{24,25} performed DPD simulation of paclitaxel loaded poly(ethylene oxide)-*b*-poly(L-lactide) PEO-*b*-PLIA in water and dimethylformamide (DMF) to observe self-assembled structures of bicontinuous, lamella, rod and spherical micelles and provided a complete phase behavior of the same system. Quite recently, it has been shown by Kriksin *et.al.*³⁵ that the local chemical structure of monomeric units can influence the global self-assembled morphology of the amphiphilic melts. It is interesting to note that so much effort has been invested to understand block copolymer assemblies, however, the explicit inclusion of charged blocks is by and large missing in most of the simulations of amphiphilic block copolymers. So far, the self-assembly of charged-neutral diblock copolymers has been studied using analytical techniques such as the random phase approximation³⁸⁻⁴⁰ (RPA), the SCFT⁴⁰ and the MC.²⁹ In MC studies,²⁹ only the thermodynamics of the system have been investigated due to the equilibrium limitations of the Monte Carlo technique which may do justice to understand the morphologies but lacks a thorough investigation that include dynamics. Only recently, experiments⁴¹ have been performed to understand the microphase separation in the charged-neutral diblock copolymer melts. Theoretically, it has been predicted that the entropic cost of confining the counterions to charged domains as a result of microphase separation stabilizes the disordered phase against ordered ones for a large parameter range. Furthermore, the morphology diagram is highly asymmetric and the regime of stability of the lamellar phase gets enhanced. We must point out here that in the field theoretical models,³⁸⁻⁴⁰ possibility of counterion adsorption⁴²⁻⁴⁵ with the lowering of the temperature was not considered and hence, the models ignore the effect of ion pair formation and their implications on the structure. This, in turn, limits the applicability of the field theoretical models without ion-pair formation to high temperature regime close to the disorder-order transition.

In this article, we investigate the dynamics and self-assembly of charged diblock copolymers at nanoscale. The diblock copolymers consist of a charged block and an uncharged block. We are interested in the morphology and dynamics of charged block copolymers near the melt monomer density. Simulation of more realistic conditions requires an ‘explicit’ presence of the charge-counterion interactions. In order to allow for an efficient simulation but account for explicit

Coulomb interactions between the charges we employ a Brownian dynamics (BD) technique with Kremer-Grest bead spring model polymer to understand the structural as well as dynamical properties of the system and investigate the parameter space to identify the most important physics issues. The interplay between the entropy of the system and electrostatic energy between the charged monomers causes the formation of specific morphologies. We have observed that the diblocks of 50% charge states on the charged block of an amphiphile forms structures that are quite different from their neutral counterpart. The chain swelling and other thermodynamic properties show the system does not follow the normal polyelectrolyte behaviors either. Similar results have been observed in recent experimental investigations^{11,21,46} for sulfonated polystyrene (sPS) and fluorinated polyisoprene (fPI) diblock copolymers. These new classes of charged block copolymers show promising new directions to understand and thereby fabricate novel functional materials which can be applicable to rather diverse applications from drug delivery to molecular electronics. The paper is organized as follows: Next section describes the simulation methodologies taking into account both Lennard-Jones (LJ) and Coulomb interactions. The relevancy of different parameters used in this simulation is explained in this section too. The results are discussed in third section and compared with existing simulation and experimental results. In section, we conclude with a short description of the major findings and their importance to novel material designing.

Simulation Method

We used Brownian Dynamics (BD) simulations to examine the morphology and dynamics of charged block copolymer chains in a melt of density, $\rho = 0.7/\sigma^3$. The simulations are performed for two different system of sizes $V = 16 \times 16 \times 16\sigma^3$ and $2V = 20.16 \times 20.16 \times 20.16\sigma^3$. For both the systems chain length of $N = 64$ is used. Each chain contains 75% uncharged block and 25% charged block. The charged block has 8 charges of charge $+q$ on it, giving a 50% degree of ionization on the backbone. The charges interact via Coulomb forces with equal number of counterions randomly dispersed in the system. The initial configuration of the model system is randomly

generated at the melt density. All the monomers in the system have mass m_i and Lennard-Jones diameter, σ . Polymer chains are modeled following the Kremer-Grest bead spring polymer model⁴⁷ in which bonded beads are connected by finitely extensible nonlinear elastic (FENE) springs represented by,

$$U_{ij}^{\text{FENE}} = -0.5kR_0^2 \ln \left[1 - \left(\frac{r_{ij}}{R_0} \right)^2 \right] \quad (1)$$

where $R_0 = 1.5\sigma$ is a finite extensibility and the spring constant, $k = 37.5\varepsilon/\sigma^2$, σ being the monomer diameter. The FENE potential in combination with the (excluded volume) repulsive interaction creates a potential well for the flexible bonds that maintain the topology of the molecules. The energetic interaction between the beads is modeled by a truncated and shifted Lennard-Jones potential. The repulsive part of the potential is given by,

$$U_{ij}^{\text{LJ}} = 4\varepsilon_R \left[\left(\frac{\sigma}{r_{ij}} \right)^{12} - \left(\frac{\sigma}{r_{ij}} \right)^6 + 1 \right], \quad r_{ij} \leq 2^{1/6}\sigma \\ = 0, \quad r_{ij} > 2^{1/6}\sigma \quad (2)$$

And the attractive part of the potential is given by,

$$U_{ij}^{\text{LJ}} = 4\varepsilon_A \left[\left(\frac{\sigma}{r_{ij}} \right)^{12} - \left(\frac{\sigma}{r_{ij}} \right)^6 + 1 \right], \quad r_{ij} \leq 2.5\sigma \\ = 0, \quad r_{ij} > 2.5\sigma \quad (3)$$

where and r_{ij} is the distance between two monomers and ε_R and ε_A are the repulsive and attractive energy parameters respectively for two different interactions described below. Each monomer of the system interacts via a short-range repulsive potential whose interaction strength, $\varepsilon \approx \varepsilon_R = 1.0$. The short-range repulsive LJ potential is shifted and truncated with a cut-off distance, $r_{ij}^R \leq 2^{1/6}\sigma$. In addition to this repulsive interactions, blocks A-A and B-B are attractive to each other with interaction strengths, $\varepsilon_{AA} = 2.0$ and $\varepsilon_{BB} = 4.0$ respectively. The above choice derives from the fact that the natural tendency of the different blocks of a BCP is to avoid each other because of the presence of dispersive intermolecular forces which often results in similar blocks

more attractive to each other than the dissimilar monomers.⁴⁸ The cross interactions for A-B with strength, ϵ_{AB} , are then obtained using Lorentz-Berthelot mixing rules. The repulsive cutoff is used in conjunction with the attractive cutoffs for the AA and BB interactions with a cut-off distance, $r_{ij}^{\text{attractive}} \leq 2.5\sigma$. As the focus of this paper is to observe the effect of electrostatics and entropy on the self-assembly and dynamics of the chains, we vary the temperature of the system along with the electrostatic parameters.

The long-range interactions between the charges on the chain and the counterions are modeled using explicit Coulomb potential,

$$U_{ij}^C = \frac{q_i q_j}{D r_{ij}} \quad (4)$$

where D is the dielectric constant of the medium. D may not be constant throughout the system if dielectric mismatch is considered, however, for the purpose of this paper D is assumed to be spatially constant. Long range Coulomb interactions are accounted for through the Ewald sum.⁴⁹ Temperature is the energy scale parameter that is varied for different sets of simulations. We introduce a second energy scale parameter which is the ratio of Coulomb and Lennard-Jones interactions: $\xi_B = q^2 / (D\sigma\epsilon_R)$. For real experimental systems, $\xi_B \sim 1-100$: we use two values of $\xi_B = 2$ and 10. The parameter ξ_B is proportional to the Bjerrum length, l_B and is a constant.

The dynamics of the monomers are governed by the classical Newton-Langevin equation,

$$m_i \frac{d\vec{v}_i}{dt} = -\vec{\nabla} U_i - \Gamma \frac{d\vec{r}_i}{dt} + \vec{W}_i(t) \quad (5)$$

where U_i is the net potential energy experienced by particle i and m_i is its mass. Γ is the friction coefficient between the chain monomer and background solvent. $\vec{W}_i(t)$ represents a Gaussian ‘white noise’ with zero mean acting on each particle.^{50,51} The last two terms couple the system to a heat-bath where the ‘friction term’ acts as a heat sink and the ‘noise term’ acts as a heat source. The first advantage of this scheme is that the natural MD integration time-steps are larger, thereby permitting simulation on longer time scales. A second advantage comes from the fact that on this time-scale, only the mean effect of the stochastic forces acting on the system needs to be con-

sidered, leading to the first order temperature relaxation law which in turn reduces the need of an external thermostat. The dimensionless units are defined as follows, $t^* = t / \sqrt{m_i \sigma^2 / \epsilon_R}$, $\rho^* = \rho \sigma^3$, $T^* = k_B T / \epsilon$, $U^* = U / k_B T$ and $r^* = r / \sigma$.

Results and Discussion

In earlier studies,^{29,46} we have demonstrated that controllable morphologies can be achieved by changing charge states of the charged diblock copolymer or by changing the dielectric constant of the solvent. In an attempt to establish a connection between thermodynamics to the dynamics of the system, we have performed a detailed molecular dynamics simulation of charged polymer and investigate the dynamics of the BCP and counterions for different thermodynamic parameters. To understand the system size effect we studied two systems, V and $2V$ described earlier. We also have varied the Coulomb energy parameter, ξ_B . The interaction parameter, ξ_B is inversely proportional to the dielectric constant, therefore $\xi_B = 10.0$ and 2.0 are used to represent low and high dielectric constant systems respectively. The system size effect is studied for $\xi_B = 10$ cases only.

[Figure 1 about here.]

[figure][1][1] shows the morphologies of the block copolymer melt for $2V$ system at $\xi_B = 10$. In these figures, the conventional diblock morphology as expected from the phase behavior of neutral block copolymers cannot be observed. From the morphology diagram for neutral diblock copolymers,^{1,2} it is well established that the neutral counterpart of this system of 75-25 diblock would have exhibited hexagonally packed cylindrical morphology. In case of neutral diblock, the minority components form the hex structures and the majority blocks form the bulk. The presence of charge sites causes electrostatic interactions to dominate over the energetic repulsion effects between blocks that induces microphase separation in the neutral BCP. The strong electrostatic effect in the charged BCP changes the interaction energies such that the hexagonal structures cannot be observed. Lowering the temperature to $T^* = 0.3$, gives rise to ‘inverse’ morphology where the minority blocks form the structures and the majority components form the matrix ([figure][1][1](b).

At even lower temperature, $T^* = 0.05$, the cylindrical nature of the ‘inverse’ morphologies cannot be observed as can be seen in [figure][1][1(a)]. At the higher side of the temperatures, the charged blocks start to form well defined structures ([figure][1][1(c)]) that eventually settles down to entropy dominated miscible phase at very high temperature, $T^* = 1.0$ ([figure][1][1(d))). The structures seen in [figure][1][1] have also been observed in recent experiments.⁴⁶ The strong electrostatic interaction causes percolation of the charges that forms a network of charged blocks at low temperatures, giving rise to these unconventional ‘inverse’ morphologies. Furthermore, note that the counterions are confined in the charged domains for all the temperatures corresponding to the ordered morphologies, in agreement with the field theoretical calculations on similar systems.⁴⁰ The lower the entropy of the system, stronger the effect of the electrostatics, giving freedom to the uncharged block to self-assemble to novel morphologies that would not have otherwise been possible.

[Figure 2 about here.]

Snapshots for high dielectric constant at $\xi_B = 2.0$ are shown in [figure][2][2]. Interestingly these snapshots show similar behavior as neutral 75-25 diblock. At lower temperature end, in [figure][2][2(a) and (b)], the charged block (minority component) form the micro structures and the majority neutral blocks form the bulk. By increasing the temperatures the structures break down as can be seen in [figure][2][2(c) and (d)] for $T^* = 0.8$ and $T^* = 1.0$ respectively. At high dielectric constant (low ξ_B), the agglomeration of charges is more prevalent compared to low D (high ξ_B). In a recent experiment,⁴⁶ it has been shown that the long-range structures of charged diblock copolymers (sPS-fPI) breaks down by adding a trace amount of water in these system. It is well established for heterogeneous materials that an increase in dielectric constant results in a decrease in percolation and vice versa.⁵² It is interesting to observe the same physics dominating the microphase separation of macromolecules, in this case, the charged diblock copolymers. In [figure][2][2(a) and (b)], increase in dielectric constant resulted in reduced percolation thereby allowing the charges (minority charged block) to agglomerate to form the structures whereas the majority block forms the bulk. A detail discussion on agglomeration of charges will be presented

in connection with radial distribution function and fraction of free counterions later in this section. These results are in agreement with experiments⁴⁶ and the SCFT calculations⁴⁰ carried out for weakly charged diblock copolymers. The addition of water increases the dielectric constant of the system which in turn lowers the electrostatic interaction strengths by a factor of $1/D$. This makes the percolation (responsible for ‘inverse’ morphology) of charges more unstable, resulting in charge agglomeration (responsible for neutral BCP morphology) instead. Decreasing the electrostatic strength brings the system from an electrostatic energy dominated regime to an entropy dominated regime, where ion-pair formation is weaker compared to a percolated state. In the entropy dominated regime, the microphase separation is hindered by the entropic cost of partitioning of counterions in the charged domains as predicted by the SCFT calculations.⁴⁰ This also explains the breakdown/disappearance of ‘inverse’ morphologies in [figure][2][2] obtained at low ξ_B . In principle, one should obtain the ‘inverse’ morphologies even for high D ($\xi_B = 2$) medium by lowering the temperature further. However, it is extremely time consuming and hard to equilibrate the system at such low temperatures (with explicit Coulomb interactions).

[Figure 3 about here.]

In order to corroborate the idea of ion-pair formation and its implications on the morphologies, we show the counterion-counterion radial distribution function (RDF), $g(r)$, in [figure][3][3]. For a complete understanding of ion-pair formation, a discussion of the ion-counterion RDF is extremely important. Due to the lack of data of fixed charges (co-ion), the ion-counterion RDF cannot be presented in this paper. Recent work on charged polymers⁵³ shows that the counterions always pair with ions. Ion-counterion pairing is also necessary from the electrostatics point of view, although this pair formation does not guarantee local electroneutrality. In [figure][3][3(a) and (b)] the RDF for $\xi_B = 10$ and $\xi_B = 2$ are shown respectively for the system size, V . We confirmed by plotting the RDF for $2V$ system that there are no apparent system size effects which might cause substantial error in the results presented in this paper. The system size effects for the simulation model can be neglected with confidence. One of the prominent features of these radial distribution functions can be seen by comparing the RDF for different temperatures. The first peak height increases by

decreasing the temperature which represents increased agglomeration of counterions. The RDF shows a distinguishable decrease in agglomeration peak for $\xi_B = 2$ compared to $\xi_B = 10$. This represents an enhanced miscibility shown in [figure][2][2]. In [figure][3][3(a)] for low D , structures can be observed at temperatures as high as $T^* = 1.0$ which is prominent in the snapshots shown in [figure][1][1]. For $\xi_B = 2$ system, an order-to-disorder like transition can clearly be observed from the sudden decrease in the $g(r)$ peak in [figure][3][3(b)]. The transition temperature is hard to locate exactly, these plots can give a qualitative understanding of transition that is associated with charged diblock copolymers. In polymer melt, it had been shown⁵⁴ that the precise transition temperature was very hard to locate.

For the model of a continuously and uniformly charged line, the radial distribution function implicitly has two peaks, the first peak corresponds to the condensed counterions and a second peak corresponds to the Debye-Huckel peak for the uncondensed counterions. The first peak is obviously an idealization of the real structure. In [figure][3][3(a)] and (b), the appearance of two peaks in RDF at low temperatures represents the counterion adsorption behavior akin to uniformly charged polyelectrolytes. However, this is not quite true because of the presence of a longer uncharged block, electrostatics and entropy both play a major role in deciding the morphology of the charged BCP. The increase in T^* breaks the morphologies at high D ([figure][2][2]) which can also be seen in [figure][3][3(b)] where the first peak height is reduced. In [figure][3][3(a)] the peak heights are higher and represent stronger agglomeration compared to the high dielectric constant case, [figure][3][3(b)] which has lower peak heights representing a much weaker agglomeration, in this case the entropic effect is much more pronounced in forming the morphologies. In [figure][3][3(a)], the second peak becomes dominant which may result in longer inter-atomic separations in a low dielectric constant medium. The first peak in [figure][3][3(a)] begins disappearing and the majority of counterions show agglomeration at an uncondensed phase (second peak) akin to the polyelectrolyte behavior. Also at high T^* the thicker width of $g(r)$ is representative of loosely bound counterions similar to polyelectrolyte behavior.⁴³ In [figure][3][3(b)], the first peaks shift to shorter inter-atomic separations with the second peak position unchanged. For

high dielectric medium, $\xi_B = 2$, the first peak positions shift due to tighter packing. The close packing of counterions seen in [figure][3][3] can electrostatically be possible if the counterions form charge-counterion pairs. Therefore, the neutral diblock behavior of the morphologies as observed in large D ([figure][2][2]) are due to the the tightly packed charge-counterion pair at each charge site of the polymer that causes the charge sites to resemble as neutral sites. On the other hand, the presence of the second peak indicates counterion-counterion correlations that extends throughout the charged block of the chain which effectively shows apparent neutralization of the charged block. This relates quite well with the snapshots shown in [figure][1][1] and [figure][2][2]. From these morphological analysis and the structural evolutions for different dielectric constants, it can easily be concluded that at low D the charged block exhibit polyelectrolyte behavior and at high D it behaves like a neutral diblock. It should be noted that both the ξ_B studied here have explicit point charges on the minority block of the chain.

[Figure 4 about here.]

To augment the understanding of charge agglomeration, cluster size distribution is investigated. A cluster is defined to be the total number of nonbonded charges associated with ‘a’ charge within a cutoff radius r_{cut} . The cut-off radius, r_{cut} is the location of the first minimum of RDF in the maximally clustered state. The total number, N_c , of non-interacting charge sites within r_{cut} is defined as the cluster size. The probability of occurrence, $P(N_c)$, of a cluster of size N_c is computed. The probability of occurrence of cluster size $N_c = 1$, $P(1)$ is taken as the fraction of free counterions. In [figure][4][4], fraction of free counterions are plotted versus temperature for two different ξ_B . The red squares represent $\xi_B = 10$ and black circles represent $\xi_B = 2$ respectively. Small $P(1)$ reflects lower free counterions, therefore higher agglomeration. For lower temperatures, very few counterions are free. Stronger agglomeration can be observed in snapshots at lower temperatures too. There is a sharp increase of $P(1)$ at around $T^* = 0.1$ which may be associated with stronger agglomeration of charges. For $\xi_B = 10$, the red squares show more clustering (less free counterions) compared to $\xi_B = 2$. From the snapshots ([figure][1][1] and [figure][2][2]), it has been observed that low dielectric constant ($\xi_B = 10$) shows more percolation of charges thereby forming reverse

morphologies. These results are consistent with [figure][4][4] in which it can be observed the $\xi_B = 10$ forming more clusters (less free counterions). From these plots though the formation of charge multiplets cannot be guaranteed as that requires an explicit representation of the fixed charge data which is absent due to unavailability of fixed charge positions. However, agglomeration of counterions cannot be justified, from an electrostatics point of view, without the presence of opposite charges. For charged polymer systems, it has been observed earlier⁵³ that multiplets form in charge agglomeration.

[Figure 5 about here.]

From these results presented so far, it is evident that thermodynamics of the charged-neutral diblock copolymers depend strongly on the electrostatic interaction strengths. To understand the thermodynamics better we have computed the specific heat capacity (C_V) from the fluctuation-dissipation formula, $C_V = (\langle E^2 \rangle - \langle E \rangle^2)/T^{*2}$ where E is the total energy of the system and ' $\langle \rangle$ ' denotes ensemble average. [figure][5][5(a)] shows the C_V as a function of temperature for different ξ_B . For $\xi_B = 10$ (red squares), a peak in C_V is observed at around $T^* = 0.1$ at low dielectric constant. The peak is absent for $\xi_B = 2$ (black circles) at higher dielectric constant. Instead there is a sudden jump in C_V for high dielectric constant ($\xi_B = 2$) at around $T^* = 0.1$. This suggests that the charged blocks undergo self-assembly (order-to-disorder transition) at this temperature. At around this temperature, the entropy of the system decreases thereby causing an abrupt change in C_V . Typically, the appearance of a 'peak' (red squares) in C_V is often referred to as the "glass transition temperature". However, the peak observed here for $\xi_B = 10$ is not associated with a glass transition as the system cannot vitrify at this temperature and density. At $\xi_B = 10$, the self-assembly is driven by electrostatic interactions rather than by entropic interactions. Since the C_V peak occurs at low dielectric constant, it is evidently related to the formation of ion-counterion multiplets.⁵³ The multiplet formation starts occurring much earlier than this transition temperature as is evident from [figure][1][1]. This phenomenon cannot be observed at $\xi_B = 2$ as the charges are dissociated at high dielectric constant. At $\xi_B = 2$ the change in C_V comes from the conformational energy of the chain rather than the multiplet formation as is evident from the abrupt increase in

C_V at low T^* . Furthermore, the absence of an abrupt increase in C_V for $\xi_B = 10$ (low dielectric constant medium) can be attributed to the higher order nature of the transition that may be caused by strongly percolating charged blocks. We have not investigated the exact nature of this transition and leave this finer point for future work. The structures also break down at higher dielectric constant. The same phenomena has been observed in experiments⁴⁶ where an addition of small trace amount of water (increasing dielectric constant) breaks down the long range order of the charge block copolymers.

To understand the structural changes that generally affect the thermodynamics, we have computed the structural relaxation time of counterions and plotted in [figure][5][5(b)]. The first dynamical quantity in this article, the structural relaxation time is obtained from self-intermediate scattering function defined by, $S(k^*, t^*)$ where k^* is a wave vector, $k = 2\pi/l$ corresponds to the first peak distance (l) of the static structure factor, $S(k^*)$. The intermediate scattering function, $S(k^*, t^*)$ follows an exponential decay. The structural relaxation time, τ^* is represented by the value of t^* where $S(k^*, t^*)$ resumes $1/e$ times initial amplitude. The red squares and blue triangles are shown for counterions and chain center-of-mass (CM) respectively for $\xi_B = 10$, i.e., at low dielectric constant and the black circles are shown for counterions at $\xi_B = 2$. For $\xi_B = 2$, the chain CM relaxation time is not shown as the major focus of this investigation is the effect of counterion relaxation. At low dielectric constant, formation of charge multiplets does not allow the counterions relax thereby a slow relaxation can be observed (red squares). These plots show an abrupt change in τ^* at low temperature which is consistent with the C_V plot shown in [figure][5][5(a)]. For the low dielectric constant ($\xi_B = 10$), the counterions cross the chain CM at around $T^* = 0.1$, exactly the temperature at which the peak in C_V has been observed. These results support the theory that the counterions undergo a structural transition at low temperatures due to multiplet formation. Below this temperature the counterion relaxation time increases strongly, consistent with the localization of charged blocks into multiplet clusters. A similar behavior has been observed in other weakly charged systems where the transition occurs due to the formation of charge multiplets.⁵³

[Figure 6 about here.]

To understand the swelling behavior of the charged diblock copolymer for different dielectric constants, we compare the radius of gyration of the charged polymer (R_g) with that of an ideal chain, $R_{g0} = \sqrt{Nb^2/6}$, where N is the degree of polymerization and b is the monomer length. The swelling ratio, $\Theta_s = R_g/R_{g0}$ versus temperature is shown in [figure][6][6]. The ratio, Θ_s is similar around the transition temperature for both $\xi_B = 2$ (black circle) and 10 (red squares). However, beyond the transition temperature, Θ_s is slightly higher for $\xi_B = 10$ than $\xi_B = 2$. This can be explained as follows. As the dielectric constant increases ($\xi_B = 2$), swelling capability of the chain decreases which can normally happen in neutral polymers only. Therefore, the swelling phenomena of the charged BCP system for $\xi_B = 2$ may be attributed to the swelling of neutral chains. On the other hand, for polyelectrolytes, increase in dielectric constant increases swelling capability. Therefore for $\xi_B = 10$ (red squares), increase in swelling phenomena can be attributed to the polyelectrolyte behavior of the charged BCP. In these data comparatively small swelling of the chain has been observed, in some cases though, the swelling has been observed to be as much as 100 times their volume for particular classes of polyelectrolytes in low-polarity (low-dielectric constant) solvents.⁵⁵ This suggests that, although there are dissociation of counterions to break the multiplets with the increase in dielectric constant, the entropy due to the dissociation of counterions is relatively small to contribute substantially in swelling of the charged BCP. The system under consideration has only 8 charges (and 8 counterions) on the first 16 monomers of a chain of length 64. These small number of charges result in statistically smaller contribution to the entropy of dissociation, although the Coulombic interactions significantly contribute to the formation and breaking of charge agglomeration as shown in [figure][1][1] and [figure][2][2].

[Figure 7 about here.]

[Figure 8 about here.]

[figure][7][7] and [figure][8][8] show the mean-square-displacement (MSD) of the counterions and chain CM for two different ξ_B . For $\xi_B = 10$ ([figure][7][7]), only the V system is shown due to lack of data to calculate correlation in the $2V$ system, but this should not be a major concern

as there is hardly any system size effects present in these calculations. In [figure][7][7(a) and [figure][8][8] counterion motion is observed to be much faster than the chain CM motion (shown in [figure][7][7(b) and [figure][8][8(b)). At low temperatures, both counterions and chain CM show sharp decrease in their respective MSDs. Although counterions show faster motion due to their smaller size compared to the chain CM, the drop in counterion MSD is more pronounced than the chain CM at $T^* = 0.05$ and 0.1 respectively. This may be due to the stronger agglomeration of counterions that causes the counterions to be entropically unfavorable to move. For low dielectric constant, $\xi_B = 10$ ([figure][7][7(a) the low temperature counterion motions become even more sluggish. This is consistent with the earlier observation of counterions forming charge multiplets at low temperatures for high ξ_B . For $\xi_B = 2$, the counterions dissociate due to the presence of more polar medium (high dielectric constant) therefore the motion is enhanced, although slow compared to the chain CM. The sudden jump in MSD for both the chain CM and counterions for both $\xi_B = 2$ and 10 suggests a transition from the non-agglomerated state to charge agglomerated state.

Conclusion

In summary, we have simulated a system of charged block copolymers in the presence of explicit counterions. The partially charged block copolymers exhibit ‘inverse’ morphologies that have been observed in recent experiments.⁴⁶ From our results, it is evident that the design of these novel functional materials depend sensitively upon the dielectric constant of the medium, the degree of ionization and the temperature of the system. Corroborative results have been obtained experimentally⁴⁶ that addition of trace amount of water (increasing dielectric constant) changes the morphology of the diblock copolymer dramatically.

Furthermore, our results highlight the existence of two regimes in the self-assembly of charged-neutral diblock copolymers. In one regime, the self-assembly is governed by electrostatic energy and in the other regime, it is dictated by the counterion entropy affecting the morphologies and other thermodynamic properties. It is interesting to note that introducing charges on a diblock

copolymer not only changes the morphologies, it acts unfavorably for both neutral polymers and polyelectrolytes depending on the dielectric of the medium. In a low dielectric medium, the self-assembly in charged-neutral diblock is electrostatically dominated and leads to non-trivial, counter-intuitive ‘inverse’ morphologies where the minority component forms the matrix and majority forms the structures. For this system, electrostatics drive the formation of ionic multiplets which increases the relaxation time of the counterions and hence affect the dynamics of microphase separation ([figure][1][1]). For high dielectric medium, the chains form neutral BCP morphologies as can be seen in [figure][2][2]. An increase in dielectric constant shifts the system towards counterion entropy dominated regime. The counterion dominated regime also can be observed with increase in temperature. In this regime, disordered phase gets stabilized against ordered structures. These results exhibit how different the 75-25 charged BCPs are from the neutral diblocks counterparts. The swelling behavior shown in [figure][6][6] shows how different these charged BCPs are from their polyelectrolyte counterparts. The swelling of the chains, although very small, shows behavior which is opposite to polyelectrolytes swelling behavior at low D . The formation of charge multiplets in a cluster and the dissociation of counterions with decreasing dielectric constant, can be understood by observing the dynamics of counterions ([figure][7][7] and [figure][8][8]). These results are in agreement with the SCFT calculations⁴⁰ for weakly charged systems, showing the stabilization of disorder phase against ordered morphologies to avoid the entropic cost of partitioning of counterions in the charged domains. It should be noted here that a discussion on the slope of the MSD (diffusion coefficients) is missing. A detailed discussion of the diffusion coefficients of the chain CM and counterions may indeed be important to understand the effect of transport coefficients on the morphological changes for different T^* and D , however, diffusion in polymers is a subject that deserves a complete separate study.

The present structural and dynamical analysis of charged diblock polymers should be of importance for understanding the fundamental mechanisms and for designing novel materials for drug delivery^{13,14,21,24,25} and nanotechnology^{56,57} applications. Additional information of different charged states and block sizes of the charged block will further enhance the understanding and

in particular provide information for counterion transport in charged polymer films.

Acknowledgement

This work was supported by the Division of Materials Science and Engineering (DMSE), U.S. Department of Energy (DoE), Office of Basic Energy Sciences (BES) under Contract No. DEAC05-00OR22725 with UT-Battelle, LLC at Oak Ridge National Laboratory (ORNL).

References

- (1) Discher, B. M.; Won, Y.-Y.; Ege, D. S.; Lee, C.-M.; Bates, F. S.; Discher, D. E.; Hammer, D. A. *Science* **1999**, *284*, 1143.
- (2) Bates, F. S.; Fredrickson, G. H. *Annu. Rev. Phys. Chem.* **1990**, *41*, 525.
- (3) Russell, T. P. *Curr. Opin. Colloid Interface Sci.* **1996**, *1*, 107.
- (4) Bates, F. S.; Fredrickson, G. H. *Phys. Today* **1999**, *52*, 32.
- (5) Fasolka, M. J.; Mayes, A. M. *Annu. Rev. Mater. Res.* **2001**, *11*, 323.
- (6) Vriezema, D. M.; Aragonés, M. C.; Elemans, J. A. A. W.; Cornelissen, J. J. L. M.; Rowan, A. E.; Nolte, R. J. M. *Chem. Rev.* **2005**, *105*, 1445.
- (7) Zhang, X.; Rehm, S.; Safont-Sempere, M. M.; Wurthner, F. *Nat. Chem.* **2009**, *1*, 623.
- (8) Jones, R. A. L. *Faraday Discuss.* **2009**, *143*, 9.
- (9) Kim, K. T.; Cornelissen, J. J. L. M.; van Hest, R. J. M. N. J. C. M. *Adv. Mater.* **2009**, *21*, 2787.
- (10) Ariga, K.; Hill, J. P.; Lee, M. V.; Vinu, A.; Charvet, R.; Acharya, S. *Sci. Technol. Adv. Mater.* **2008**, *9*, 014109.
- (11) Li, Z.; Chen, Z.; Chu, H.; Hales, K.; Wooley, K. L.; Pochan, D. J. *Langmuir* **2007**, *23*, 4689.

- (12) Zhang, L.; Eisenberg, A. *Science* **1995**, *268*, 1728.
- (13) Gaucher, G.; Dufresne, M. H.; Sant, V. P.; Kang, N.; Maysinger, D.; Leroux, J. C. *J. Controlled Release* **2005**, *109*, 169.
- (14) Garrec, D. L.; Ranger, M.; Leroux, J. C. *Am. J. Drug Delivery* **2004**, *2*, 15.
- (15) Hu, X. L.; Jing, X. B. *Expert Opin. Drug Discovery* **2009**, *6*, 1079.
- (16) Savic, R.; Azzam, T.; Eisenberg, A.; Nedev, H.; Rosenberg, L.; Maysinger, D. *Biomaterials* **2009**, *30*, 3597.
- (17) Bajpai, A. K.; Shukla, S. K.; Bhanu, S.; Kankane, S. *Prog. Polym. Sci.* **2008**, *33*, 1088.
- (18) Beduneau, A.; Saulnier, P.; Benoit, J. P. *Biomaterials* **2007**, *28*, 4947.
- (19) Jain, S.; Bates, F. S. *Macromolecules* **2004**, *37*, 1511.
- (20) Halperin, A.; Tirrell, M.; Lodge, T. P. *Adv. Polym. Sci.* **1992**, *100*, 31.
- (21) Cui, H.; Chen, Z.; Chong, S.; Wooley, K. L.; Pochan, D. J. *Science* **2007**, *317*, 647.
- (22) Li, X. A.; Tang, P.; Qiu, F.; Zhang, H. D.; Yang, Y. L. *J. Phys. Chem B* **2006**, *110*, 2024.
- (23) Ortiz, V.; Nielson, D. E.; Discher, D. E.; Klein, M. I.; Lipowsky, R.; Shillcock, J. *J. Phys. Chem B* **2005**, *109*, 17708.
- (24) Guo, X. D.; Tan, J. P. K.; Kim, S. H.; Zhang, L. J.; Zhang, Y.; Hedrick, J. L.; Yang, Y. Y.; Qian, Y. *Biomaterials* **2009**, *30*, 6556.
- (25) Guo, X. D.; Tan, J. P. K.; Zhang, L. J.; Khan, M.; Liu, S. Q.; Yang, Y. Y.; Qian, Y. *Chem. Phys. Lett.* **2009**, *473*, 336.
- (26) Sknepnek, R.; Anderson, J. A.; Lamm, M. H.; Schmalian, J. R.; Travesset, A. *ACS Nano* **2008**, *2*, 1259.

- (27) Erdtman, E.; dos Santos, D. J. V. A.; Lofgren, L.; Eriksson, L. A. *Chem. Phys. Lett* **2008**, *463*, 178.
- (28) Srinivas, G.; Discher, D. E.; Klein, M. I. *Nat. Matter*. **2004**, *3*, 638.
- (29) Goswami, M.; Sumpter, B. G.; Mays, J. W. *Chem. Phys. Lett* **2010**, *487*, 272.
- (30) Deschenes, I.; Bousmina, M.; Ritcey, A. M. *Langmuir* **2008**, *24*, 3699.
- (31) Du, H. B.; Zhu, J. T.; Jiang, W. *J. Phys. Chem B* **2007**, *111*, 1938.
- (32) Ma, J. W.; Li, X.; Tang, P.; Yang, Y. I. *J. Phys. Chem B* **2007**, *111*, 1552.
- (33) Sevinek, G. J. A.; Zvelindovsky, A. V. *Macromolecules* **2005**, *38*, 7502.
- (34) Li, X.; Guo, J.; Liu, Y.; Liang, H. *J. Chem. Phys.* **2009**, *130*, 074908.
- (35) Kriksin, Y. A.; Khalatur, P. G.; ten Brinke, I. Y. E. G.; Khokhlov, A. R. *Soft Matter* **2009**, *5*, 2896.
- (36) Khokhlov, A. R.; Khalatur, P. G. *Chem. Phys. Lett* **2008**, *461*, 58.
- (37) Xin, J.; Liu, D.; Zhong, C. *J. Phys. Chem. B* **2009**, *113*, 9364.
- (38) Marko, J.; Rabin, Y. *Macromolecules* **1991**, *24*, 2134.
- (39) Marko, J.; Rabin, Y. *Macromolecules* **1992**, *25*, 1503.
- (40) Kumar, R.; Muthukumar, M. *J. Chem. Phys* **2007**, *126*, 214902.
- (41) Park, M.; Balsara, N. *Macromolecules* **2008**, *41*, 3678.
- (42) Manning, G. S. *J. Chem. Phys.* **1969**, *51*, 924.
- (43) Liu, S.; Muthukumar, M. *J. Chem. Phys.* **2002**, *116*, 9975.
- (44) Muthukumar, M. *J. Chem. Phys.* **2004**, *120*, 9343.

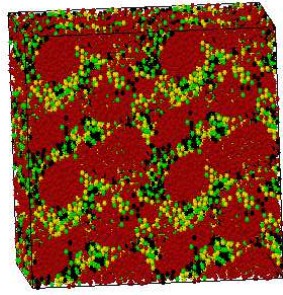
- (45) Kumar, R.; Kundagrami, A.; Muthukumar, M. *Macromolecules* **2009**, *42*, 1370.
- (46) Goswami, M.; Sumpter, B. G.; Huang, T.; Messman, J. M.; Gido, S. P.; Isaacs-Sodeye, A. I.; Mays, J. W. *Soft Matter* **2010**, DOI: 10.1039/c0sm00733a.
- (47) Kremer, K.; Grest, G. S. *J. Chem. Phys.* **1990**, *92*, 5057.
- (48) Ruzette, A.-V. *Nature Materials* **2002**, *1*, 85.
- (49) Leeuw, S. W. D. *Proc. R. Soc. London A* **1980**, *373*, 27.
- (50) van Gunsteren, W. F.; Berendsen, H. J. C. *Mol. Phys.* **1977**, *34*, 1311.
- (51) van Gunsteren, W. F.; Berendsen, H. J. C. *Mol. Phys.* **1982**, *45*, 637.
- (52) Nan, C.-W.; Shen, Y.; Ma, J. *Annu. Rev. Mater. Res.* **2010**, *40*, 131.
- (53) Goswami, M.; Kumar, S. K.; Bhattacharya, A.; Douglas, J. F. *Macromolecules* **2007**, *40*, 4113.
- (54) Wang, J. F.; Dormidontova, E. E.; Lodge, T. P. *Macromolecules* **2002**, *35*, 9687.
- (55) Ono, T.; Sugimoto, T.; Shinkai, S.; Sada, K. *Nat. Matter.* **2007**, *6*, 429.
- (56) Li, Z. B.; Kesselman, E.; Talmon, Y.; Hillmyer, M. A.; Lodge, T. P. *Science* **2004**, *306*, 98.
- (57) Lodge, T. P. *Science* **2008**, *321*, 5885.

List of Figures

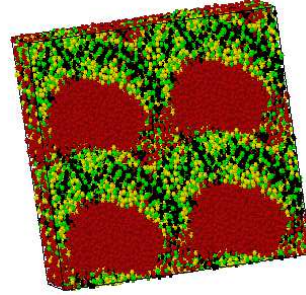
1	<p>Snapshots at the end of the simulation for different temperatures at $\xi_B = 10.0$ for $2V$ system. (a) $T^* = 0.05$, (b) $T^* = 0.3$, (c) $T^* = 0.8$ and (d) $T^* = 1.0$. The maroon represents uncharged block monomers. Black and yellow represent charged block monomers, black being the neutral monomeric unit and yellow being the charged sites of the charged block. The green dots are the counterions. The central simulation cell is repeated in all the three directions to preserve the continuity of the chains images due to the periodic boundary conditions.</p>	25
2	<p>Snapshots at the end of the simulation for different temperatures at $\xi_B = 2.0$. (a) $T^* = 0.05$, (b) $T^* = 0.1$, (c) $T^* = 0.3$ and (d) $T^* = 0.8$. The maroon represents uncharged block monomers. Black and yellow represent charged block monomers, black being the neutral monomeric unit and yellow being the charged sites of the charged block. The green dots are the counterions. The central simulation cell is repeated in all the three directions to preserve the continuity of the chains images due to the periodic boundary conditions.</p>	26
3	<p>Radial distribution function $g(r)$ of counterions for all the temperatures. The two different systems shown here are: (a) $\xi_B = 10$ at V system size and (b) $\xi_B = 2$ for V system size. For $\xi_B = 2$, more temperature data have been obtained as shown in the legend</p>	27
4	<p>Fraction of free counterions as a function of temperature for $\xi_B = 2$ (black circles) and $\xi_B = 10$ (red squares) systems. The lines in these plots are guide to the eyes.</p>	28
5	<p>Specific heat, C_V for all the temperatures $T^* = 0.05, 0.1, 0.3, 0.5, 0.8$ and 1.0. (b) Counterion structural relaxation time for $\xi_b = 10$ (red squares) and $\xi_B = 2$ (black circle). The blue triangles represent polymer center-of-mass structural relaxation time for $2V$ system at $\xi_B = 10$. At around $T^* = 0.3$ the counterion τ^* becomes stronger than the chain CM τ^*.</p>	29

6	Ratio of radius-of-gyration to the radius-of-gyration of an ideal chain of same chain length for $\xi_B = 2$ (black circles) and $\xi_B = 10$ (red squares) systems. For $\xi_B = 10$, system size $2V$ is used. $\xi_B = 10$ shows more chain swelling compared to $\xi_B = 2$. The lines are not data, these are merely guide to the eyes for the respective swelling parameters.	30
7	Mean square displacement at $\xi_B = 10.0$ for (a) counterions and (b) chain center-of-mass. Black line represent $T^* = 0.05$, red line 0.1, green line 0.3, blue line 0.5, magenta line 0.8 and cyan line 1.0 respectively. MSD is shown for V system due to lack of data for $2 \times V$ system.	31
8	Mean square displacement at $\xi_B = 2.0$ for (a) counterions and (b) chain center-of-mass. Respective temperatures for the lines are shown in the legends.	32

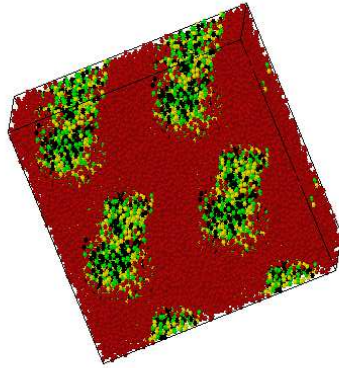
List of Figures



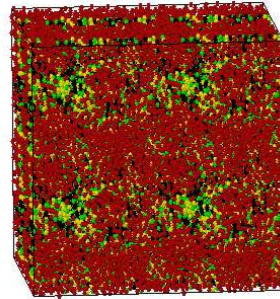
(a) $T^* = 0.05$



(b) $T^* = 0.3$

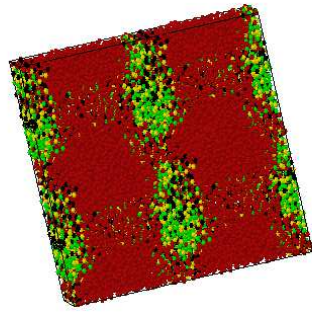


(c) $T^* = 0.8$

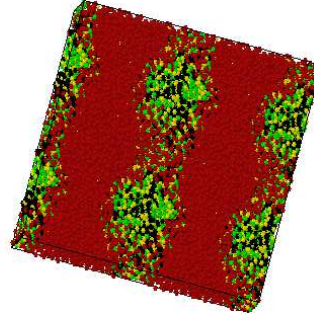


(d) $T^* = 1.0$

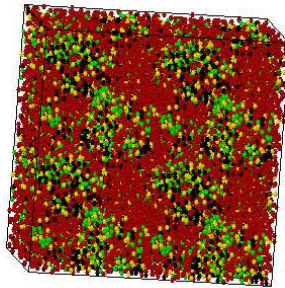
Figure 1: Snapshots at the end of the simulation for different temperatures at $\xi_B = 10.0$ for $2V$ system. (a) $T^* = 0.05$, (b) $T^* = 0.3$, (c) $T^* = 0.8$ and (d) $T^* = 1.0$. The maroon represents uncharged block monomers. Black and yellow represent charged block monomers, black being the neutral monomeric unit and yellow being the charged sites of the charged block. The green dots are the counterions. The central simulation cell is repeated in all the three directions to preserve the continuity of the chains images due to the periodic boundary conditions.



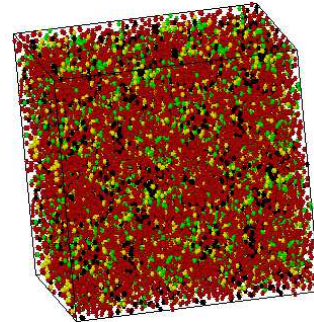
(a) $T^* = 0.05$



(b) $T^* = 0.1$

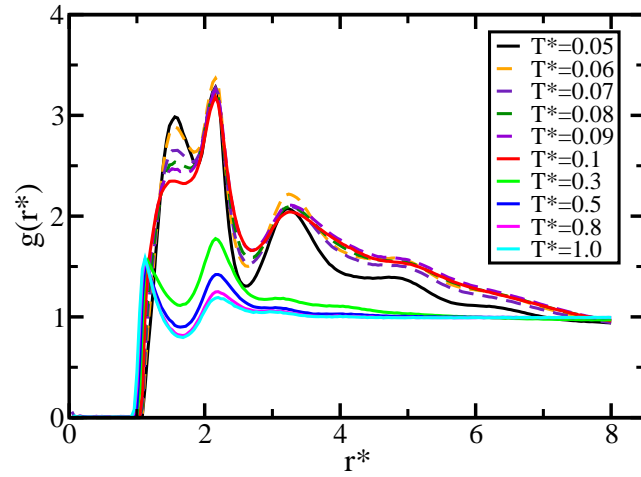
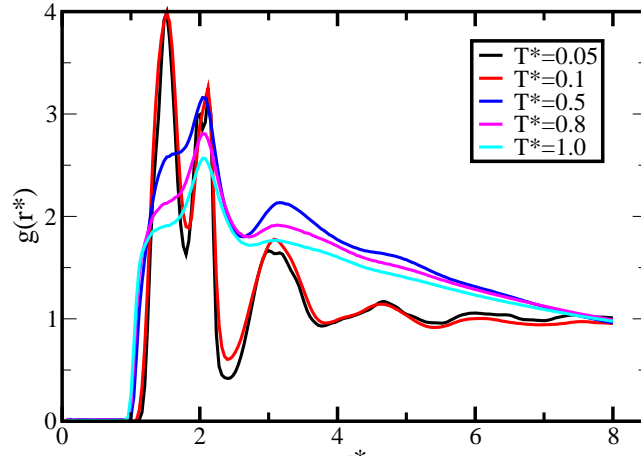


(c) $T^* = 0.3$



(d) $T^* = 0.8$

Figure 2: Snapshots at the end of the simulation for different temperatures at $\xi_B = 2.0$. (a) $T^* = 0.05$, (b) $T^* = 0.1$, (c) $T^* = 0.3$ and (d) $T^* = 0.8$. The maroon represents uncharged block monomers. Black and yellow represent charged block monomers, black being the neutral monomeric unit and yellow being the charged sites of the charged block. The green dots are the counterions. The central simulation cell is repeated in all the three directions to preserve the continuity of the chains images due to the periodic boundary conditions.



(b) $\xi_B = 2$

Figure 3: Radial distribution function $g(r)$ of counterions for all the temperatures. The two different systems shown here are: (a) $\xi_B = 10$ at V system size and (b) $\xi_B = 2$ for V system size. For $\xi_B = 2$, more temperature data have been obtained as shown in the legend

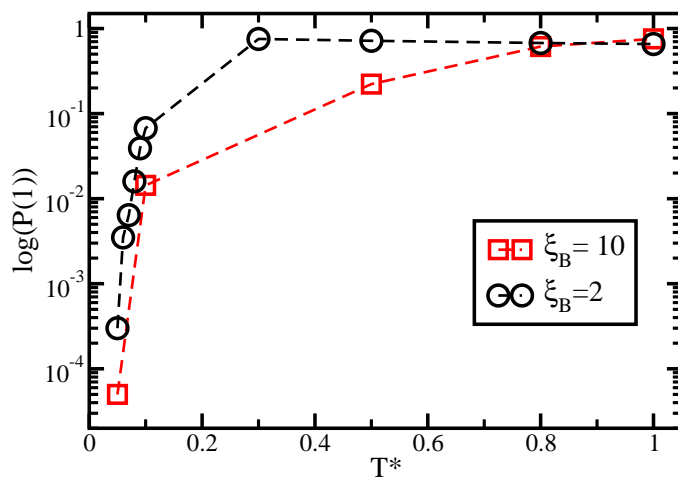
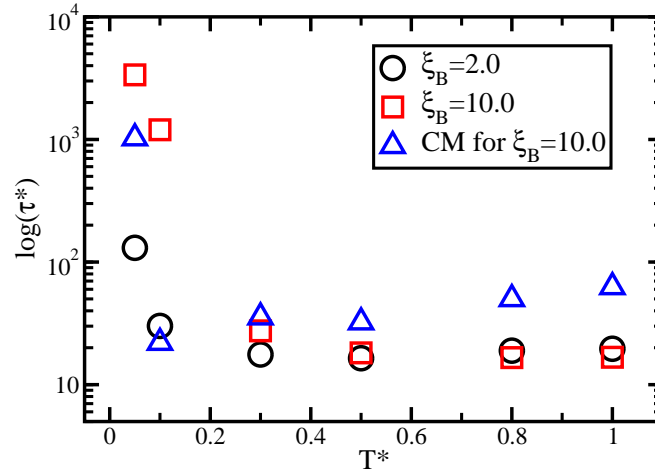
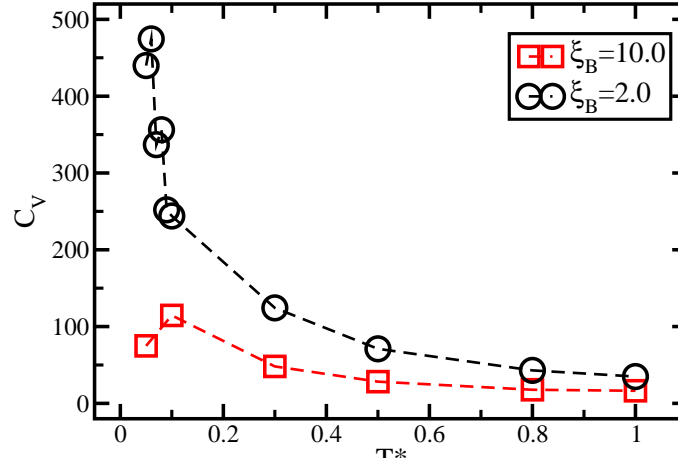


Figure 4: Fraction of free counterions as a function of temperature for $\xi_B = 2$ (black circles) and $\xi_B = 10$ (red squares) systems. The lines in these plots are guide to the eyes.



(b) Structural relaxation time

Figure 5: Specific heat, C_V for all the temperatures $T^* = 0.05, 0.1, 0.3, 0.5, 0.8$ and 1.0 . (b) Counterion structural relaxation time for $\xi_b = 10$ (red squares) and $\xi_B = 2$ (black circle). The blue triangles represent polymer center-of-mass structural relaxation time for $2V$ system at $\xi_B = 10$. At around $T^* = 0.3$ the counterion τ^* becomes stronger than the chain CM τ^* .

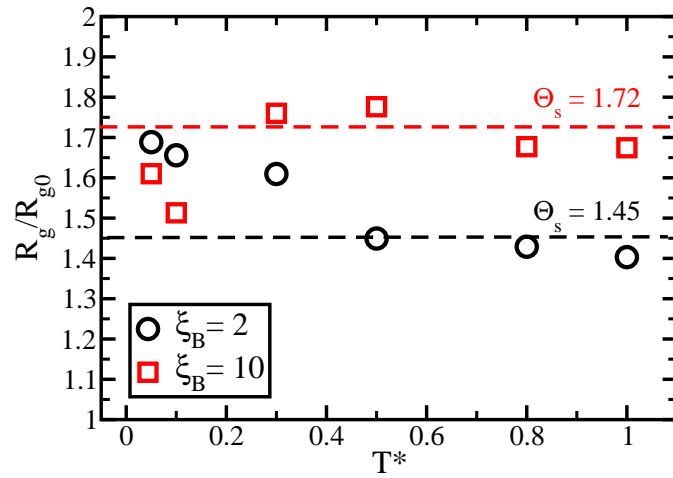
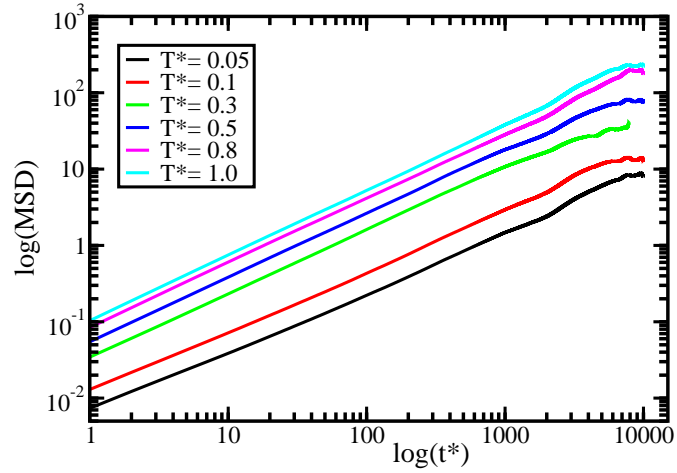
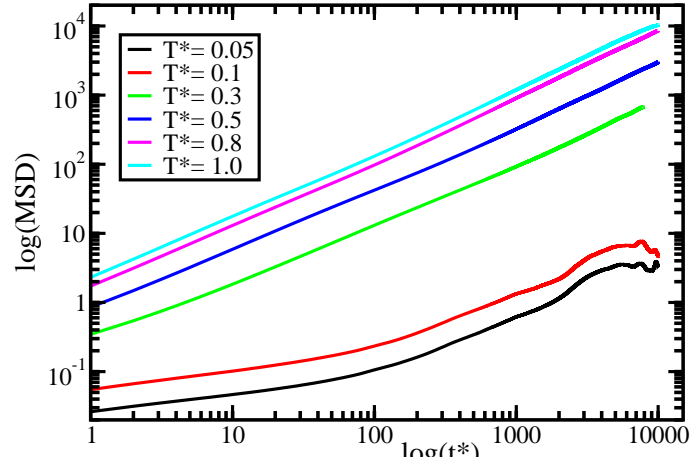


Figure 6: Ratio of radius-of-gyration to the radius-of-gyration of an ideal chain of same chain length for $\xi_B = 2$ (black circles) and $\xi_B = 10$ (red squares) systems. For $\xi_B = 10$, system size $2V$ is used. $\xi_B = 10$ shows more chain swelling compared to $\xi_B = 2$. The lines are not data, these are merely guide to the eyes for the respective swelling parameters.



(b) Chain CM MSD

Figure 7: Mean square displacement at $\xi_B = 10.0$ for (a) counterions and (b) chain center-of-mass. Black line represent $T^* = 0.05$, red line 0.1, green line 0.3, blue line 0.5, magenta line 0.8 and cyan line 1.0 respectively. MSD is shown for V system due to lack of data for $2 \times V$ system.

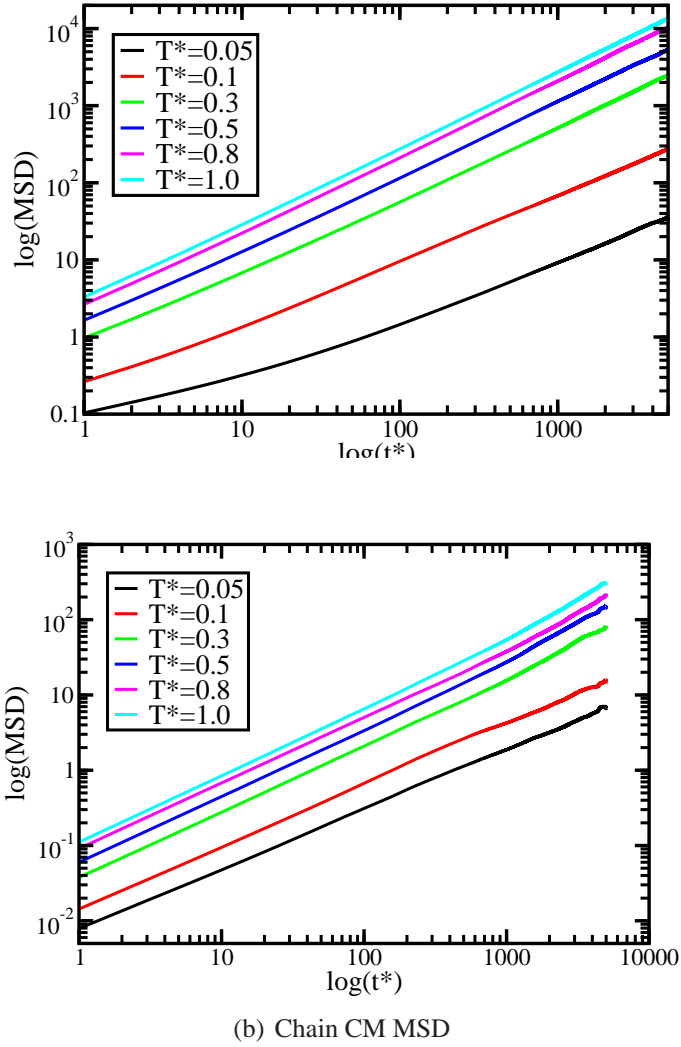


Figure 8: Mean square displacement at $\xi_B = 2.0$ for (a) counterions and (b) chain center-of-mass. Respective temperatures for the lines are shown in the legends.